Effects of a Brueckner–Hartree–Fock Corrected Effective Mass on Speed of Sound, Conformality, and Observables of Dark Matter–Admixed Neutron Stars

Arijit Das[1] Prashanth Jaikumar[2] Adarsh Karekkat[1,3] Tanumoy Mandal[1]

[1] IISER Thiruvananthapuram, Vithura, Kerala 695 551, India
[2] California State University Long Beach, Long Beach, California 90840, USA
[3] Université de Caen Normandie, ENSICAEN, CNRS/IN2P3, LPC Caen UMR6534, F-14000 Caen, France

Physical Review C **112**, 055803 (2025)

Neutron Stars as Astrophysical Laboratories

- Neutron stars (NSs) serve as a natural laboratory for strongly interacting matter at supernuclear densities
- Observational probes:
  - Gravitational waves (GW170817, GW190425)
  - Pulsar data for PSR J0740+6620, PSR J0030+0451 etc.
- Challenge: Neither pQCD nor lattice QCD applies at intermediate baryon densities $2\rho_0$–$5\rho_0$, ρ_0 being the nuclear saturation density.
- **Relativistic Mean-Field (RMF)** models: fitted to nuclear saturation properties

Key Limitations of Standard RMF

- Many-body forces neglected
- Often fail to reach $\sim 2M_\odot$ for certain parameter sets

This Work

Incorporate **BHF-informed** nucleon effective masses into an RMF framework with **fermionic dark matter**

Motivation: Why BHF Effective Mass?

Standard RMF

- Effective nucleon mass m_N^* obtained from self-consistent solutions of field equations
- Misses microscopic three-body forces
- Three-body interactions key to achieving $M_{\max} \gtrsim 2M_\odot$

BHF Framework

- Relativistic BHF includes 2-body as well as 3-body nuclear potentials
- Provides density-dependent effective-mass ratio $Y_{\mathrm{BHF}}(\rho_V)$
- *External input* to solve the EoMs.

Goals of this work

1. Study effects on NS mass-radius, compactness, tidal deformability, moment of inertia
2. Examine **speed of sound** profile and **conformality** indicators
3. Explore **dark matter (DM) admixed** neutron stars (DMANS)

Model: Dark Matter Admixed SU(2) Chiral Sigma Model

Total Lagrangian

$$\mathcal{L} = \mathcal{L}_H + \mathcal{L}_{DM} + \mathcal{L}_I$$

Hadronic sector $\mathcal{L}_H$:

- SU(2) nucleon doublet ψ
- Mesons: σ, π, ω, ρ
- Scalar potential $U(\bar{x}) = \frac{\lambda}{4}\bar{x}^4 + \frac{B}{6}\bar{x}^6 + \frac{C}{8}\bar{x}^8$ where $\bar{x}^2 = \sigma^2 - x_0^2$

Dark Matter $\mathcal{L}_{DM}$:

- Fermionic DM spinor χ, mass m_χ
- Scalar mediator ϕ, vector mediator ξ
- DM parameters constrained using relic density and DM self interaction cross-sections.

Interaction $\mathcal{L}_I$:

$$-g_\phi \bar{\psi}\psi\phi - g_\xi \bar{\psi}\gamma^\mu\psi\xi_\mu - y_\phi \bar{\chi}\chi\phi - y_\xi \bar{\chi}\gamma^\mu\chi\xi_\mu$$

Effective masses in RMF:

$$m_N^* = g_\sigma\sigma + g_\phi\phi, \quad m_\chi^* = m_\chi + y_\phi\phi$$

Parameter Fitting for Hadronic Sector

Hadronic params fitted to SNM:
$\rho_0 = 0.153\ \text{fm}^{-3}$, $K = 231\ \text{MeV}$,
$E_B/A = -16.3\ \text{MeV}$

BHF Effective-Mass Ratio: Analytical Fit

BHF fitting function (Shang et al. 2020):

$$Y_{\rm BHF} = a_1 + b_1\beta + c_1\beta^2 + (a_2 + b_2\beta + c_2\beta^2)\rho_V + \frac{d_1}{\rho_V} + d_4 \ln \rho_V$$

The asymmetry parameter $\beta = 1$ for purely neutron matter.

BHF scenario:

- Replace $m_n^* \to Y_{\rm BHF}\, m_n$ in the EoM for σ
- Solve for $\phi_{\rm BHF}(\rho_V) \Rightarrow$ modified m_χ^*
- BHF mass ratio $Y_{\rm BHF}$ deviates significantly from $Y_{\rm RMF}$.
- At low $\mathcal{E}$, crust matching using BSK19.

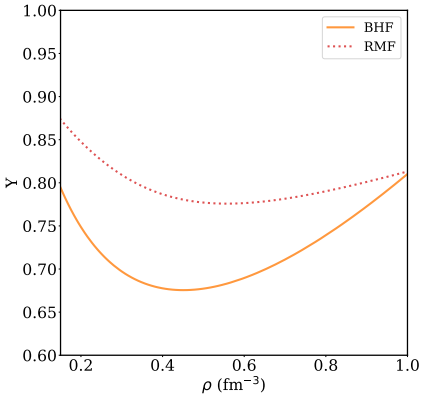

Figure: Comparison of RMF and BHF corrected nucleon effective-mass ratios for purely hadronic EoS

Equation of State: RMF vs BHF

EoS comparison (BP II shown):

- Both RMF and BHF EoSs satisfy the constraint $\Lambda_{1.4} < 400$ (Annala et al. 2018).
- The BHF EoS is stiffer at low density and softer at high density compared to RMF.
- The slope of the BHF EoS is consistent with trends observed in various RMF EoSs in the literature (Xia et al. 2022).
- Regions excluded by the RKT condition

$$P < 3\left(\rho^V m_n^\star + \rho_\chi^V m_\chi^\star + \mathcal{E}\right)$$

  lie well above the EoS curves.
- Non-monotonic slope of BHF EoS alludes to the non-monotonic profile of C_S^2.

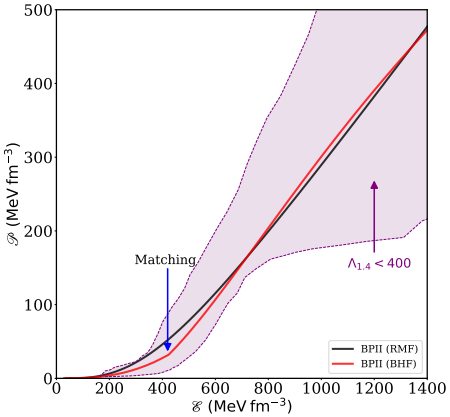

Figure: RMF and BHF EoSs for BP II.

Mass-Radius Relations: RMF vs BHF

RMF scenario:

- $M_{\max} \approx 2.00$–$2.13\, M_\odot$
- Consistent with PSR J0740+6620, GW190425; Radius at $1.4\, M_\odot$: $\sim$ 12–13 km

BHF scenario:

- $M_{\max} \approx 1.93$–$2.03\, M_\odot$
- Tighter M-R curves; radius ~ 10.9 km
- Better agreement with HESS J1731-347, PSR J1231-1411, PSR J0437-4715, *Tension* with PSR J0740+6620 and GW190425 M_1
- BHF radius *less sensitive* to m_χ than RMF
- Fall within $\Lambda(1.4\, M_\odot) < 400$, consistent with GW170817 constraints

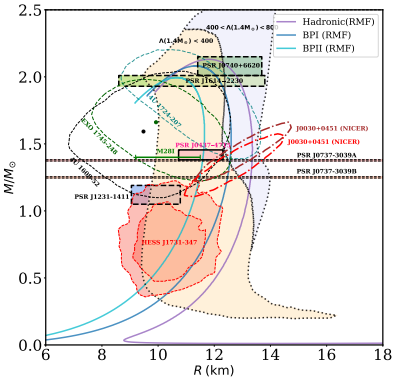

Figure: Mass-radius relationships for hadronic, BPI, and BPII parameters in the RMF scenario.

Mass-Radius Relations: RMF vs BHF

RMF scenario:

- $M_{\max} \approx 2.00$–$2.13\, M_\odot$
- Consistent with PSR J0740+6620, GW190425; Radius at $1.4\, M_\odot$: $\sim$ 12–13 km

BHF scenario:

- $M_{\max} \approx 1.93$–$2.03\, M_\odot$
- Tighter M-R curves; radius ~ 10.9 km
- Better agreement with HESS J1731-347, PSR J1231-1411, PSR J0437-4715, *Tension* with PSR J0740+6620 and GW190425 M_1
- BHF radius *less sensitive* to m_χ than RMF
- Fall within $\Lambda(1.4\, M_\odot) < 400$, consistent with GW170817 constraints

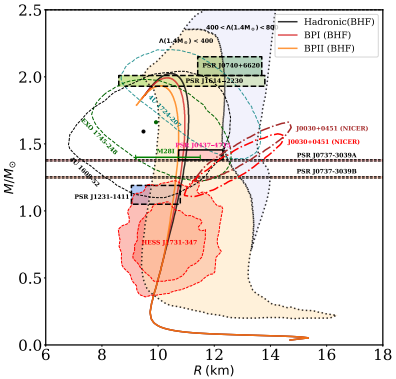

Figure: Mass-radius relationships for hadronic, BPI, and BPII parameters in the BHF scenario.

Tidal Deformability ($\Lambda_{1.4}$): RMF vs BHF

BHF reduces $\Lambda_{1.4}$

- BHF $\Lambda_{1.4}$ not consistent with joint analysis of GW170817 and PSR J0030+0451 but consistent with GW170817 alone ((70–580)).
- BHF results are much less sensitive to variations of m_χ.
- Tidal deformability significantly reduced: $\Lambda_{1.4} : 532 \to 134$ (Hadronic) and $\Lambda_{1.4}^{\mathrm{BHF}} : 134 \to 109$ (BP II).

Dark Matter Sensitivity

- $\Lambda_{1.4}^{\mathrm{BHF}} : 134 \to 109 \quad (19\%)$
- $\Lambda_{1.4}^{\mathrm{RMF}} : 532 \to 336 \quad (37\%)$

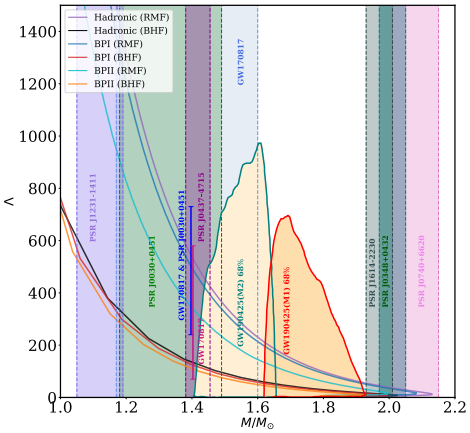

Figure: RMF and BHF tidal deformability.

Compactness & Moment of Inertia

Compactness $C = GM/c^2R$:

- BHF: C increases nearly linearly with M (narrow radius range $R \approx 10.9$ km)
- RMF: broader range consistent with PSR J0030+0451 mass/compactness
- BHF mass inferred from J0030+0451 compactness: $(1.03\text{–}1.19)M_\odot$ — lower than observed

Moment of Inertia I (slow-rotation):

- $I_{\rm BHF}/I_{\rm RMF} \approx 0.68$ at $M = 1.4M_\odot$
- BHF consistent with PSR J0737-3039A (light double pulsar)

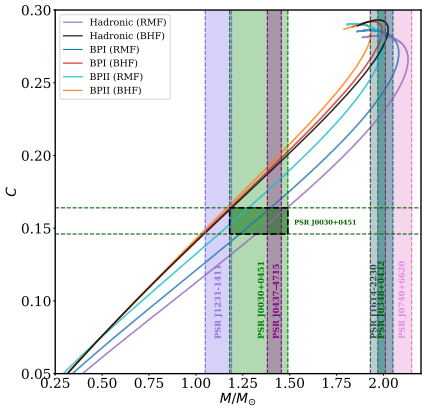

Figure: M-C relations for RMF and BHF cases.

Compactness & Moment of Inertia

Compactness $C = GM/c^2R$:

- BHF: C increases nearly linearly with M (narrow radius range $R \approx 10.9$ km)
- RMF: broader range consistent with PSR J0030+0451 mass/compactness
- BHF mass inferred from J0030+0451 compactness: $(1.03\text{–}1.19)M_\odot$ — lower than observed

Moment of Inertia I (slow-rotation):

- $I_{\rm BHF}/I_{\rm RMF} \approx 0.68$ at $M = 1.4M_\odot$
- BHF consistent with PSR J0737-3039A (light double pulsar)

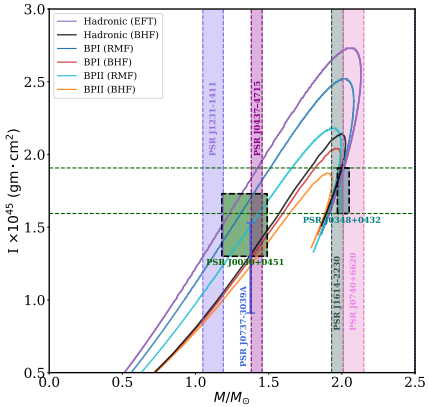

Figure: M-I relations for RMF and BHF cases.

Speed of Sound: $C_S^2 = \partial P / \partial \mathcal{E}$

RMF scenario:

- Monotonically increasing C_S^2
- Exceeds conformal limit $1/3$ at intermediate ρ_V
- Does not return toward $1/3$ at high density

BHF scenario:

- Nonmonotonic C_S^2: rises, peaks, then approaches the conformal limit
- Approaches conformal limit at $\rho_V \approx 1.05\ \mathrm{fm}^{-3} \approx 7\rho_0$
- Lies within 1σ confidence band (Marczenko et al. 2024) for $\rho_V \approx 0.6$–$1.05\ \mathrm{fm}^{-3}$
- Approach toward conformal limit at high density may signal transition to weakly coupled quark matter (Gorda et al. 2018, 2021)

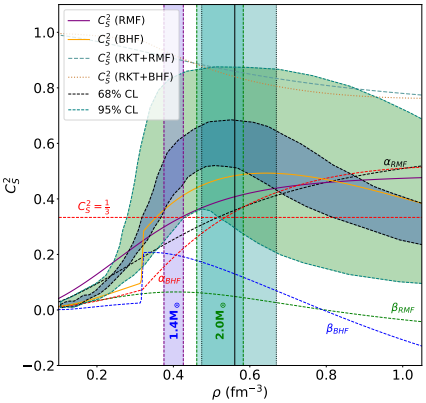

Figure: C_S^2 profile as a function of ρ.

Conformality Indicators

Multiple measures of conformality:

1. **Trace anomaly** $\Delta = \frac{1}{3} - \frac{P}{\mathcal{E}}$:
$\Delta = 0$ in conformal limit
2. **Speed of sound decomposition** $C_S^2 = \alpha + \beta$:

$$\alpha = \frac{2\rho}{\mu}\frac{d(\mathcal{E}/\rho)}{d\rho}, \quad \beta = C_S^2 - \alpha$$

Conformality onset: $\beta \approx 0$
BHF: better agreement with 1σ limits for $\rho_V \in [0.3, 0.8]$ fm^{-3}

3. **Conformal Distance**

$$d_c = \sqrt{(1/3 - \langle C_S^2 \rangle)^2 + (C_S^2 - \langle C_S^2 \rangle)^2}$$

$d_c \to 0$ in conformal limit; onset ≈ 0.2

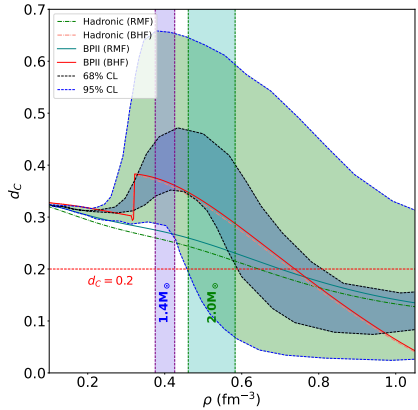

Figure: d_C as a function of ρ

Finite-Temperature Extension: Isentropic DMANS (Under Progress)

Warm Dark Matter Admixed Neutron Stars

- Proto-neutron stars evolve approximately under **constant entropy per baryon** $s = s_0$
- Self-consistent RMF solutions determine $T = T(s_0, \rho_B)$ as well as $\rho_\chi(s_0, \rho_B)$.
- DM chemical potential treated as a free parameter $\kappa = \mu_\chi / M_\chi$.
- Matter composition:$npe\chi$ under charge neutrality and β equilibrium.
- Finite entropy heats the stellar core, while dark matter admixture tries to cool it, leading to competing thermal and dark-sector effects.

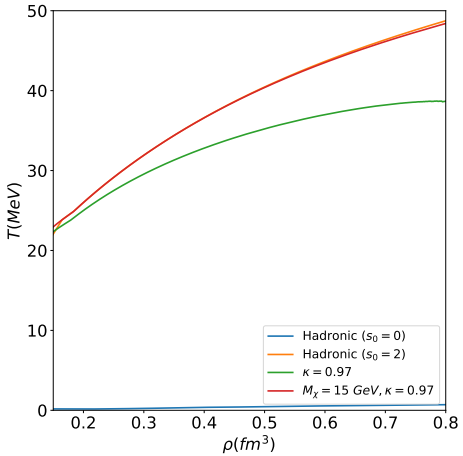

Figure: Self-consistent temperature profiles.

Competition Between Thermal Effects and Dark Matter

Thermal Effects vs DM Softening

- Increasing entropy s_0 increases the maximum mass of NS.
- Inclusion of DM $\Longrightarrow$ Amplified DM density profiles for increasing s_0 $\Longrightarrow$ Gradual softening of the EoS $\Longrightarrow$ Reduction of M_{Max}
- Larger κ enhances DM density near the stellar core.
- Lighter DM particles induce stronger softening $\longrightarrow$ Aggressive softening of the EoS.
- The macroscopic properties of warm DMANS are governed by the competition between these two effects.

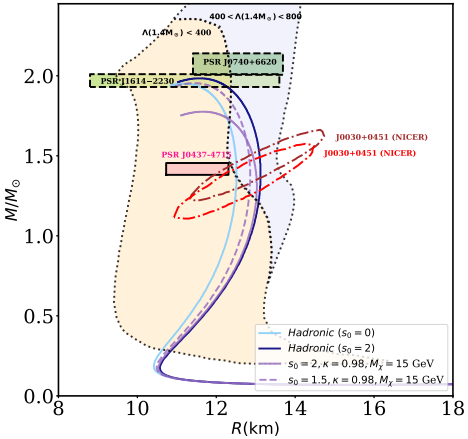

Figure: Mass-radius relations for varying κ.

Speed of Sound Profile

Conformality in Neutron-Star Interiors

- Conformal threshold: $C_S^2 = \frac{1}{3}$.
- For sufficient amount of DM in the NS core, the C_S^2 profile can develop a non-monotonic profile.

Key Message

[Thermal effects $\Longleftrightarrow$ DM softening]

The onset of conformality inside neutron stars is governed by the competition between these two effects.

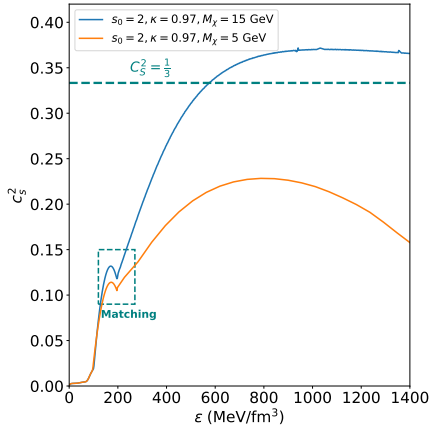

Figure: Non-monotonicity of the speed of sound profile.

Thank You!

Questions?

Arijit Das
IISER Thiruvananthapuram

arijit21@iisertvm.ac.in

Backup: TOV Equations & Macroscopic Observables I

Tolman–Oppenheimer–Volkoff (TOV) equations:

$$\frac{dP}{dr} = -(\mathcal{E} + P)\frac{M + 4\pi r^3 P}{r(r - 2M)}, \qquad \frac{dM}{dr} = 4\pi r^2 \mathcal{E}$$

Moment of Inertia (slow-rotation, Hartle 1967):

$$\frac{1}{r^4}\frac{d}{dr}\left[r^4 j(r)\frac{d\bar{\omega}}{dr}\right] + \frac{4}{r}\frac{dj}{dr}\bar{\omega} = 0, \qquad I = \frac{c^2}{6G}\frac{R^4}{\Omega(R)}\left.\frac{d\bar{\omega}}{dr}\right|_{r=R}$$

Tidal Love number k_2 and deformability:

$$\Lambda = \frac{2}{3}k_2 C^{-5}, \qquad C = \frac{GM}{c^2 R}$$

k_2 computed from perturbation of the metric, solving a Riccati ODE for $y(r)$ with $y(0) = 2$.

Backup: Observed Pulsar Data Used

Object	$M/M_\odot$	R (km)	Λ	I (10^{45} g cm^2)
PSR J0030+0451	$1.34^{+0.15}_{-0.16}$	$12.71^{+1.14}_{-1.19}$	370^{+360}_{-130}	$1.43^{+0.30}_{-0.13}$
PSR J0348+0432	1.97–2.05	12.16–12.95	—	1.594–1.907
PSR J0740+6620	2.08 ± 0.07	$12.39^{+1.30}_{-0.98}$	—	$4.65^{+1.16}_{-0.82}$
PSR J0437–4715	1.418 ± 0.037	$11.36^{+0.95}_{-0.63}$	—	—
PSR J1231–1411	1.12 ± 0.07	$9.91^{+0.88}_{-0.86}$	—	—
PSR J0737-3039 A	1.377 ± 0.005	8.14–25.74	—	$1.15^{+0.38}_{-0.24}$
GW170817	1.17–1.60	11.9 ± 1.4	70–580	—
GW190425	1.12–2.52	—	$1.4^{+3.8}_{-1.2} \times 10^3$	—

Backup: DM Parameter Sets

Set	m_χ	m_ϕ	m_ξ	$y_\phi = y_\xi$	$g_\phi = g_\xi$
BP I	5 GeV	9 MeV	11 MeV	0.13	1.1×10^{-4}
BP II	15 GeV	20 MeV	34 MeV	0.21	1.1×10^{-4}

- Parameters consistent with **Bullet Cluster** self-interaction constraints and thermal relic DM abundance
- Small $g_{\phi,\xi}$ ensures DM-nucleon scattering cross-section within experimental bounds
- Purely neutron matter + DM (no protons or leptons) to isolate BHF effects